Three-dimensional laser creation of a Near-IR laser-gain medium based on hydride donor/acceptor complexes made of coupled laser-induced silver nanoclusters with ytterbium ions

Fouad Alassani, Guillaume Raffy, Mathis Carpentier, Joëlle Harb, Véronique Jubera, André del Guerzo, Lionel Canioni, Thierry Cardinal, Yannick Petit

Three-dimensional laser creation of near-IR laser-gain medium based on hydride donor/acceptor complexes made of coupled laser-induced silver nanoclusters with Ytterbium ions

*Fouad Alassani,[1] Guillaume Raffy,[2] Mathis Carpentier,[1] Joëlle Harb,[1] Véronique Jubera,[1] André Del Guerzo,[2] Lionel Canioni,[1] Thierry Cardinal,[1] Yannick Petit[1,]**

[1] *Université de Bordeaux, CNRS, Bordeaux INP, ICMCB, UMR 5026, F-33600, Pessac, France.*

[2] *Université de Bordeaux, CNRS, Institute of Molecular Sciences (ISM, UMR 5255), F-33400, Talence, France.*

Keywords: fluorescent silver nanocluster, direct laser writing, energy transfer, sub-diffraction limit, rare earth co-doping, hybrid systems, laser active media

Corresponding author : yannick.petit@u-bordeaux.fr

Abstract : Femtosecond laser inscription in a Ytterbium-doped silver-containing phosphate glass is demonstrated, by achieving 3D highly-localized laser-induced silver photochemistry. The produced fluorescent silver nanoclusters lead to high optical contrast in the visible range, showing that the co-insertion of Yb^{3+} ions is not detrimental to the silver-based photochemistry. We demonstrate efficient energy transfer from these silver nanoclusters to the rare earth Yb^{3+} ions, leading to a near-IR background-free fluorescence emission. Indeed, we demonstrate the 3D-localized near-IR emission of homogeneously-distributed Yb^{3+} ions thanks to their spatially-selective excitation by co-localized silver nanoclusters. This creation of hybrid donor/acceptor systems, composed of coupled laser-inscribed silver nanoclusters and Yb^{3+} ions respectively, allows for the 3D-distribubed creation of laser-active gain medium. The reported effective laser gain results from the silver nanocluster mediated excitation of the Yb^{3+} lasing ions, demonstrating the energy transfer-based achievement of inversion population and optically-induced transparency of the material. This opens the route for the all-optical fabrication of near-IR micron-scale multiscale architectures compatible with the development of new laser active media especially for integrated waveguides and active photonic integrated circuits. This includes perspectives of versatile 3D laser integrated architectures allowing for evanescent coupling under lasing operation

with their environment, to achieve enhanced photonic sensing abilities beyond those offered by usual conventional planar of unidirectional architectures.

1. Introduction

For the two last decades, femtosecond laser modifications of dielectric materials have allowed for an incredibly rich panel of local behaviors under laser/matter interaction and resulting multiscale photonic architectures, taking place in an extremely large scope of materials since multi-photon absorption and resulting femtosecond Direct Laser Writing (DLW) offers the unique opportunity to design highly-localized intra-volume modifications[1,2]. Nowadays, this gives birth to mature approaches compatible with industrial transfers for breakthrough photonic devices including analogical quantum simulators based on photonic integrated circuits (PIC)[3], opto-mechanical or sensing devices[4,5], femtosecond fiber lasers[6,7], perennial multi-dimensional high-density optical data storage[8], high-precision optical standards for the complete calibration of confocal fluorescence microscopes[9], multiple waveguiding components[10,11] or all-optically produced integrated laser waveguides[12,13].

In the case of integrated laser waveguides, the active gain medium is initially present and femtosecond laser inscription provides the additional smooth refractive index modifications needed for the creation of the waveguiding structure[10]. It appears appealing if femtosecond laser inscription could provide both the formation of the waveguiding structure and the lasing active behavior. Such an objective would require either to fully create the spectroscopic scheme compatible with laser amplification or emission, or alternatively to modify an existing lasing medium. The formation of donor/acceptor pairs is of interest for the design of efficient laser emitting systems by decoupling the absorption and emission phenomena and insuring energy from the donor to the acceptor as in Ytterbium-Erbium amplifiers and lasers[14]. A large literature reports on the role of silver species in glassy materials for enhancing the luminescence of co-inserted RE elements, by means of surface plasmon enhancement and/or energy transfers[15]. Indeed, energy transfers from silver nanoclusters to Yb^{3+} have been evidenced ions in oxifluoride glass[16,17] and in borosilicate or germanate[18,19] glasses. Still, such RE fluorescence enhancement is always randomly distributed in the material's bulk and controlled spatial distribution of the luminescence properties remains challenging.

In this framework, we have demonstrated in the past few years that femtosecond direct laser writing in silver-containing photosensitive glasses allows for the unique activation of silver photochemistry, leading thus to the creation of highly-localized distributions of fluorescent silver nanoclusters at the root of a broadband range of applications[26,27]. These new molecular species are located on each side of the laser-irradiated tracks, leading to double-track 3D fluorescent structures. The phenomenon has been numerically modeled in detail to describe the free electron trapping by Ag^{+} ions and the formation of mobile Ag^{0} species, the thermal and silver species diffusions as well as the growth of silver nanoclusters from the mobile Ag^{0} species[28,29]. In this sense, laser-induced photochemistry is very general as it can address a broad variety of glasses such as various phosphate compositions (insertion during the synthesis process)[28] or commercial glasses such as borosilicate or sodocalicite glasses (injection by ion exchange after the synthesis)[29]. We recently took benefits of the refractive index (Δn) modulation associated to sub-micron fluorescence tracks to produce sub-wavelength refractive periodicities (down to 200 nm) leading to Gaussian-like single-mode guided profiles[30] as well as the creation of high-efficiency first-order integrated waveguide Bragg gratings[31]. Such photo-induced silver-based Δn modification has been labelled Type A (A for *Argentum*): it specifically depicts the locally-induced changes of polarizability associated with the creation of the molecular silver nanoclusters, without affecting the glass matrix[32,33]. Still, despite the achievements in both visible fluorescence and refractive index patterning, the inscription of 3D luminescent patterns in the near-IR remains challenging. Novel approaches, based on our photosensitive glasses, is required to access on-demand 3D-distributed fabrication of near-IR emitters and integrated laser active waveguides.

In this article, we demonstrate laser writing of silver nanocluster in the volume of a silver and ytterbium co-doped phosphate glass. The micron-scale 3D-localised patterns exhibit high luminescence contrast properties in the visible and the near IR range. We investigate energy transfers from laser-induced silver molecular species to Yb^{3+} ions using detailed fluorescence lifetime imaging microscopy. Then we investigate the behavior of laser-inscribed laser gain properties, namely of laser-inscribed laser gain medium, which is very uncommon to the best of our knowledge[34]. In this framework, the present work demonstrates for the first time, that 3D-localized laser-inscribed acceptor/donor complexes can be created on-demand and that the resulting energy transfer can be considered for the optical pumping of the created laser gain

medium. This brings a much broader versatility in terms of photonic architecture development compared to standard homogeneously (co-)doped planar of unidirectional laser media. Thus, laser amplification in a laser-inscribed waveguided configuration has been characterized.

2. Results and Discussion

2.1 Femtosecond laser inscription of 3D visible and near-IR luminescence

A series of patterns inscribed at fixed femtosecond laser irradiance of 7.93 TW.cm^{-2} and constant sample speed of 50 µm.s^{-1}, while varying the inter-line between two successive laser passes from 10 µm down to 250 nm, have been induced in silver and ytterbium co-doped phosphate glass. These inter-line between two successive laser passes were chosen to be respectively larger or smaller than the typical dimension of laser/glass interaction voxel, in order to investigate the potential overwriting effects on nanoclusters-to-Yb^{3+} energy transfers. Thus Fig. 1(a) displays the hyperspectral fluorescence images of the laser-inscribed patterns associated to the laser-created molecular silvers nanoclusters Ag_m^{x+} (with typical nuclearities $m < 10$ and charges $x < m$)[35-37]. Indeed, the molecular silver nanoclusters result from aggregation of few silver atom Ag^0 (considered as electron trapped center[38]), and silver ions Ag^+, with good stability both thermal (below $T_g \sim 400$°C here) and over time (possibly over more than a decade[39], as shown in accelerated thermal ageing approaches[40]). As reported in the review article[28], the highly-localized photo-activation of silver chemistry in such a glass as well as the creation of new molecular silver nanoclusters located at each side of the laser/glass voxel during sample translation[26-29,37], is preserved despite the insertion of Yb^{3+} ions at this doping level. The direct excitation of these molecular silver near visible, where the Yb^{3+} absorption is quite null, promotes both visible (from silver nanocluster Ag_m^{x+}) and near-IR emission (from Yb^{3+}), demonstrating the co-localised emission of these species (Ag_m^{x+} and Yb^{3+}). Thus, energy transfer phenomenon from Ag_m^{x+} to Yb^{3+} allows a background free double track fluorescence in visible and near-IR as shown in Fig. S1.

Figure 1(b) shows that fluorescence spectra (recorded from the visible to the near IR) for an excitation at 473 nm exhibit similar profile whatever the inter-distances between successive laser passes[35-37]. For a single laser pass, the fluorescent double-track profile typically shows a typical

separation of 1.8 µm corresponding to the voxel parameter. For inter-distances of 10 µm to 5 µm, successive laser passes do not overlap. For an inter-distance of 1 µm, successive laser passes overlap once, which globally leads to a more intense fluorescent pattern, as shown with the orange to red curves in Fig. 1(b). However, while reducing the inter-distance between successive laser passes below 1 µm down to 250 nm (namely much below the voxel diameter of 1.8 µm), the spatially-integrated fluorescence amplitude globally decreases both for the silver nanocluster emission in the visible and for the Yb^{3+} ions emission in the near-IR range. However, after normalizing the fluorescence spectra per amount of fluorescent lines, the fluorescence amplitude per silver nanocluster track appears to decrease as soon as there is spatial overlap between successive laser passes, as shown in Fig. 1(c, left vertical axis). Nevertheless, the 1 µm separation pattern appears as being the brightest pattern as it behaves as an optimal situation. Indeed, the 1 µm pattern appears globally brighter than the 5 µm pattern because the increase of density of fluorescent lines of the 1 µm pattern dominates its associated drop of efficiency per fluorescent line compared to that of the 5 µm pattern. Moreover, the 1 µm pattern appears globally brighter than the 0.5 µm and 0.25 patterns because the increase of density of fluorescent lines of the 0.5 and 0.25 µm patterns is dominated by their drop of efficiency per fluorescent line compared to that of the 1 µm pattern. In this context, the decrease of the visible emission reveals a global decrease of the amount of the considered fluorescent silver nanoclusters being excited at 473 nm per line. A corresponding decrease of the non-normalized near-IR emission appears. The fluorescence amplitude ratio of the near-IR fluorescence emission (from the Yb^{3+} ions) with respect to the visible silver nanocluster emission has been estimated, as shown in Fig. 1(c, right vertical axis). One observes a reasonably constant ratio from no overlapping to moderately overlapping cases with inter-distances down to 0.5 µm (with a moderate ration increase of ~12 % at 1 µm inter-distances). Such moderate overlap situations depict the correlation and the rather linear dependence between the emission amplitudes in the near-IR and in the visible ranges. For the strong overlapping case with inter-distances of 0.25 µm, the fluorescence ratio drops by about 28 %, possibly indicating the creation of partially different populations of silver nanoclusters allowing less energy transfers to the ytterbium ions. Horizontal dashed lines in Fig. 1(c) are guide lines for the eye that indicate the range of laser inter-distances without overlapping so that both the integrated visible fluorescence intensity and near-IR/visible fluorescence ratio are expected to be constant. Still, since

the Yb^{3+} ions show a background-free near-IR emission under excitation at 473 nm one can conclude that such an Yb^{3+} excitation is selective to the silver nanocluster excitation in the laser-structured glass system under study. Such a background-free near-IR Yb^{3+} emission (strictly co-located with the laser-inscribed silver clusters) ensures that their direct excitation from the existing virtual level centered at 490 nm can be excluded here. As the observed near-IR emission is mostly proportional to that of the silver nanocluster emission, this implies that the Yb^{3+} excitation is totally mediated by the excited silver nanoclusters, which demonstrates energy transfer from these laser-induced silver species to the Yb^{3+} ions. As visible in Fig. 1(d), such an energy transfer is strictly co-localized with the laser-induced silver nanoclusters, allowing thus for a 3D-localized near-IR emission despite the homogeneous spatial distribution of these near-IR emitters.

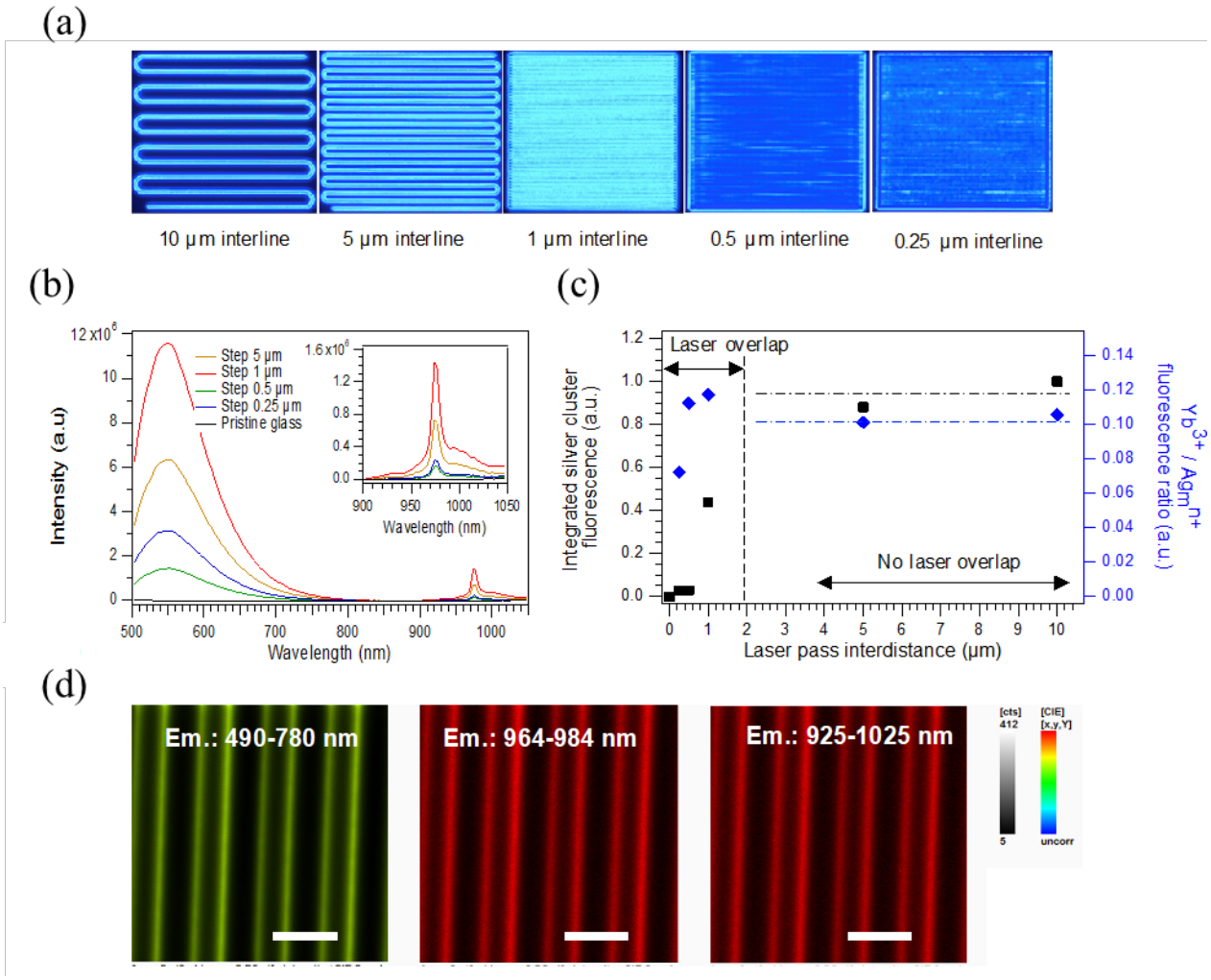

Three-dimensional laser creation of near-IR laser-gain medium based on hydride donor/acceptor complexes made of coupled laser-induced silver nanoclusters with Ytterbium ions © 2024 by Fouad Alassani, Guillaume Raffy, Mathis Carpentier, Joëlle Harb, Véronique Jubera, André Del Guerzo, Lionel Canioni, Thierry Cardinal, Yannick Petit is licensed under CC BY-ND 4.0

Figure 1. (a) Laser inscription of fluorescent patterns with various separations from 10 µm down to 250 nm between two successive laser passes, at fixed velocity of 50 µm.s^{-1} and fixed irradiance of 7.93 TW/cm^2. (b) Fluorescence spectra under cw excitation at 473 nm versus the laser pass periodicity for an identical region of interest, showing non-normalized identical fluorescence profiles (obvious when spectra are normalized) but amplitude dependence both in the visible and near-IR ranges. (c) Integrated silver nanocluster fluorescence normalized per of fluorescent line between 400 nm and 900 nm showing a decay when laser overlap occurs (left vertical scale), and fluorescence amplitude ratio between near-IR Yb^{3+} emission and visible silver nanoclusters emission (right vertical scale) showing a reasonnable correlation and linearity betwwen these two types of emission from distinct emitters although a significant decrease occurs at small interline separations of 0.25 µm. Vertical dashed line shows the typical separation with/without overlap; horizontal dashed lines are guide line for the eye to show where values are explexted to remain constant in absence of laser overlap.(d) Confocal hyperspectral background-free fluorescence image under cw 473 nm excitation, collected either for the visible silver nanocluster emission range or for the near-IR Yb^{3+} emission around its zero-phonon line emission, respectively. Scale bar : 5 µm.

From abovementioned result (as illustrated in Fig.1) the addition of these Yb^{3+} ions (2% molar amount) did not affect the laser inscription process so that very similar silver-based photochemistry was equally activated in both the Yb^{3+}-containing and Yb^{3+}-free glasses(seen Fig. 2a), leading to bright fluorescent molecular silver nanoclusters. Thus, Yb^{3+} ions, being homogeneously distributed in the pristine glass, provides additional spectroscopic properties, namely the usual UV charge transfer band and the electronic dipolar near-IR absorption and emission 4f-4f transitions.

For excitation at 473 nm as clearly well-illustrated in Figs. 1(a,b), only the laser irradiated area displays a near-IR emission. This remarkably demonstrates the ability to achieve background-free highly-localized near-IR emission below the diffraction limit under visible excitation, despite the homogeneous random distribution of the Yb^{3+} near-IR emitters, in the glass[43]. Such background-free 3D-localized near-IR emission results on the spectroscopically-selective direct excitation of highly-localized silvers nanoclusters while no Yb^{3+} ions absorption band exist in the visible range. Such an observation of background-free indirect excitation of the co-inserted rare earth elements and their subsequent localized emission provides a new milestone in the local laser-induced management of spectroscopic properties of glassy materials. Indeed, in our previous work in silver-Europium co-doped photosensitive glasses, we had reported a 5-fold enhancement of the Eu^{3+} emission co-located with laser-inscribed silver nanoclusters since Eu^{3+} ions display many absorption bands in the visible range allowing direct excitation of the rare earth[44].

The co-localized silver nanoclusters and Yb^{3+} ions behave thus as a pair of donor-acceptor with the presence of energy transfer from silver nanoclusters to Yb^{3+} ions. Such energy transfer is first corroborated by the background-free typical near-IR emission of Yb^{3+} ions, which covers all the possible Stark components of the rare earth $^2F_{5/2} \rightarrow {}^2F_{7/2}$ transitions. Silver nanocluster

fluorescence visible emission and subsequent Yb^{3+} near-IR emission, shown in Fig. 1(c,d), are be perfectly co-localized, which proves that the Ag_m^{n+} → Yb^{3+} energy transfer takes place strictly at the location of the laser-inscribed silver nanoclusters. A linear dependence of the near-IR Yb^{3+} emission with the visible Ag_m^{n+} emission is evidenced (Fig. 1(c)), whatever the laser inscription parameters. This excludes any long-range radiative process that would couple Ag_m^{n+} nanoclusters to Yb^{3+} ions by means of re-absorption processes over the whole sample.

2.2 Confocal fluorescence lifetime imaging of laser-inscribed patterns with distinct inter-distances

The spatially-selective activation of near-IR emission of the randomly-distributed Yb^{3+} ions is made possible by means of the selective excitation of 3D-localized laser-inscribed silver nanoclusters for excitation wavelengths out of the Yb^{3+} absorption bands[43]. Similarly to what observed with other rare earth ions (namely Eu^{3+} ions)[44], the final demonstration of energy transfer from the excited silver nanoclusters to the Yb^{3+} ions requires to investigate the energy transfer from silver nanoclusters to Yb^{3+} ions. Thus, fluorescence lifetime of silver nanocluster was conducted on both Yb^{3+}-free and Yb^{3+}-doped silver phosphate glasses. The experiment was performed by collecting emission of silver nanoclusters over the spectral range of 400–600 nm. Excitation was achieved with a UV 375 nm pulsed laser (approximately 120 ps, 5 MHz). Even if 375 nm excitation can also provide a direct excitation of the Yb^{3+} ions, their near-IR emission was both filtered out spectrally in the collected visible range and temporally in the nanosecond range since the fluorescence lifetime of the silver nanoclusters is not affected by the millisecond-scale lifetime of the near-IR Yb^{3+} fluorescence emission[43]. In other words, the collected decay measurements strictly correspond to contributions from the silver nanoclusters. In this framework, Figs. 2(a) and 2(b) show a composite image build of regions of interest collected by FAST- Fluorescence Lifetime Imaging Microscopy (FAST-FLIM) of the laser-inscribed patterns for different inter-distance between successive laser passes (from Fig. 1(a)) for both silver phosphate and Ag-Yb phosphate glasses. All these FAST-FLIM images show the same spatial scale, where the color code and the brightness depict the pixel-to-pixel FAST-FLIM average lifetime and the associated fluorescence intensity, respectively. For both the silver phosphate and Ag-Yb phosphate glasses, the FAST-FLIM images corroborate the double-line spatial distribution of laser-induced fluorescent silver

nanoclusters for laser pass inter-distances larger than the voxel size (inter-distances of 10 µm and 5 µm, as shown in Fig. 2(a)). For both samples, the 1 µm inter-distance leads to a well-defined 1D-array of fluorescent lines with 1 µm separation resulting from one single overlap between successive laser passes. For the 0.5 µm inter-distance, one observes a still well-defined but less intense 1D-array of fluorescent lines with 0.5 µm separation resulting from multiple overlaps between successive laser passes. Finally, the 0.25 µm inter-distance leads to a much less contrasted and even less intense 1D-array of fluorescent lines. Such an apparent loss of the fluorescence contrast originates from different aspects : (i) the involved concentration of silver nanoclusters showing excitation at 375 nm decreases after multiple overlaps between successive laser passes; (ii) the spatial quality of the 1D array may be affected by any precision lack during the sample's translation during the laser inscription process while considering small periodicities down to 250 nm; and (iii) the fluorescent periodicity becomes similar or even lower that the experimental resolution of the confocal hyperspectral microscope.

The intensity-weighted FAST-FLIM lifetime histograms were extracted from Figs. 2(a) and 2(b) for each pattern with varying inter-distances between successive laser passes. The case of the 5 µm inter-distance separation is reported in Fig. 2(c) for both the silver phosphate and Ag-Yb phosphate glasses, which highlights the lifetime shortening of silver nanocluster emission in the presence of Yb^{3+} ions. These histograms clearly show the mean lifetime shortening of the silver nanocluster excited states in the presence of Yb^{3+} ions, with a typical peak value of the histograms occurring at a shorter lifetime of 4.4 ns for the Ag-Yb phosphate glass, compared to the 5.6 ns lifetime for the silver phosphate glass. Therefore, the Yb^{3+} ions presence affects the emission rate of the neighboring silver nanoclusters, leading to a partial quenching by energy transfer.

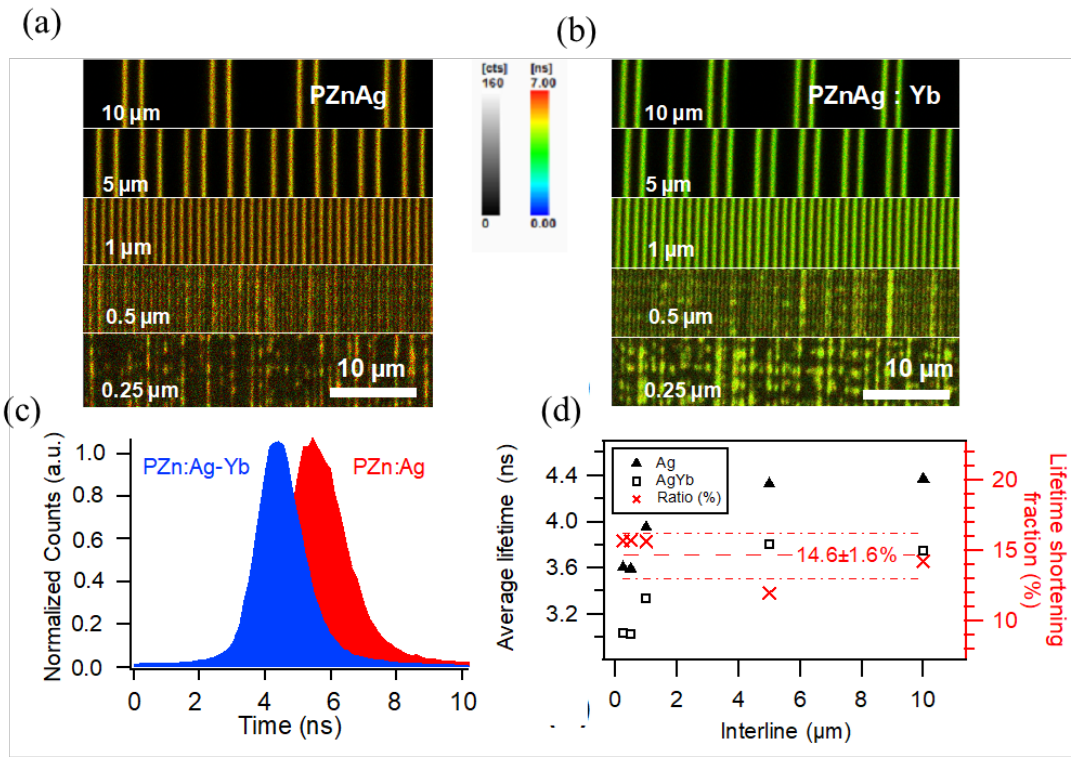

Figure 2. (a,b) Composite images for the 5 periodicity-dependent patterns of series #2 made of confocal FLIM imaging in samples PZnAg and PZnAg:Yb, respectively (excitation at 375 nm with a 120-ps source at 5 MHz, collection over the whole visible spectral range of silver nanocluster emission), showing both grey-scale intensimetric and colorimetric lifetime scales (scale bar 5 µm). (c) Intensity-weighted lifetime histograms from FAST-FLIM analysis for the PZnAg and PZnAg:Yb glasses obtained from FLIM images depicted in Figs. 2(a) and 2(b), respectively, for the case of the 5 µm period separation, showing the lifetime reduction of silver nanocluster emission. (d) Fluorescence lifetime for each of the 5 periodicity-dependent patterns from Figs. 2(a) and 2(b), respectively, and associated lifetime relative shortening due to the insertion of Yb^{3+} ions. Scale bar : 10 µm.

Laser-induced silver nanocluster distributions are dependent on laser irradiation parameters. The associated fluorescence emission shows a broad multi-band spectrum over the whole visible range[26,45]. Thus, fluorescence lifetime was evaluated with a multiple exponential decay model in the sub-ns and ns range. Such a phenomenological multi-exponential decay model gave access to a better statistics by performing curve fitting on decays that result from the binning of pixels of larger regions of interest. Note that this model does not depict the intrinsic nature and concentration of fluorescent silver species, but it handles with the complexity of the lifetime decay in order to estimate the average decay time, taking into account the statistical characteristics of single photon counting. The chosen fitting model was a three-exponential decay, as it is consistent with previous fitting results in similar silver-containing glass[26] while fitting with two- or four exponential decays

was generally either non-sufficient or non-necessary. Fluorescence decays for each condition of Figs. 2(a,b) are shown in Fig. S3, and fitting results are gathered in Table 1. The dominant time τ_2 around 3 ns is in agreement with what reported elsewhere[26], while the time τ_1 around 6 ns is analog to what observed recently[44]. The shorter time τ_3 around 1 ns was also typically observed[26,44]. The involved fitted times and associated weights gathered in Table 1 are plotted in Fig. S4, emphasizing on the overall consistency of the whole fitted parameters. Due to the multi-physics laser-induced material modification, the creation of various silver nanoclusters with distinct concentrations varies with distinct focusing conditions so that it is reasonable that the estimated lifetimes can slightly vary between distinct experimental conditions.

Based on the fitting parameters, the amplitude-weighted average emission lifetime $\tau^{ampl} = \sum_i A_i\tau_i / \sum_i A_i$ were estimated for both the silver phosphate and Ag-Yb phosphate glass samples, for each inter-distance between successive laser passes. This led to values depicted in Fig. 2(d), with various noticeable aspects. First, the amplitude-weighted average emission lifetime τ^{ampl} is always shorter for Ag-Yb phosphate than for silver phosphate glass. Second, such lifetimes tend to get longer, from 3.1 ns up to 3.8 ns for Ag-Yb phosphate and from 3.6 ns up to 4.4 ns for silver phosphate, while reducing the inter-distance between laser passes, which suggests that the nature and/or environment of silver nanoclusters differs when overwriting occurs. Third, it appears that the lifetime shortening of the amplitude-weighted average emission lifetimes of Ag-Yb phosphate ($\tau^{ampl}_{Ag,Yb^{3+}}$) with respect to that of silver phosphate (τ^{ampl}_{Ag}) corresponds to the same typical shortening of 14.6±1.6 % whatever the considered inter-distance between laser passes. This 14.6±1.6 % average relative lifetime shortening was systematically calculated by the amplitude-weighted quenching rate $Q_{\tau^{ampl}_{Ag,Yb^{3+}}/\ \tau^{ampl}_{Ag}} = 1 - \tau^{ampl}_{Ag,Yb^{3+}}/\ \tau^{ampl}_{Ag}$, which characterizes the efficiency of energy transfer[46,47]. This suggests thus that the nonradiative energy transfer process is maintained without being significantly affected by the modifications of the nature and/or environment of silver nanoclusters when laser overlapping occurs for inter-distance between laser passes smaller that the voxel size of 1.8 µm.

Composition	Interline (μm)	A_1 (%)	τ_1 (ns)	A_2 (%)	τ_2 (ns)	A_3 (%)	τ_3 (ns)	τ^{amp} (ns)
AgYb	10	15.9	6.54	50.3	3.26	33.8	1.06	3.04
	5	14.8	6.60	50.8	3.30	34.3	1.08	3.06
	1	16.1	6.72	54.2	3.49	29.7	1.20	3.33
	0.5	16.5	6.93	58.8	3.92	24.7	1.47	3.81
	0.25	22.9	6.53	56.4	3.51	20.7	1.25	3.76
Ag	10	23.8	6.70	55.0	3.24	21.1	1.07	3.60
	5	16.3	7.28	55.5	3.63	28.2	1.36	3.59
	1	13.6	7.85	60.1	4.08	26.3	1.63	3.95
	0.5	16.9	7.73	62.2	4.21	20.8	1.90	4.32
	0.25	25.9	7.19	60.4	3.78	13.7	1.61	4.36

Table 1. Fit parameters of multi-exponential decays of the normalized fluorescence decays of both the PZnAg and PZnAg:Yb glasses, from data obtained with a 375 nm pulse excitation of 120 ps at 5 MHz, and a collection range in the 400-600 nm spectral range.

Indeed, the Ag_m^{n+} → Yb^{3+} energy transfer is experimentally signed with the clear lifetime shortening in the visible range of the Ag_m^{n+} nanoclusters. In presence of Yb^{3+} the decrease of the peak position of the single-photon time resolved emission spectroscopy from 5.6 ns to 4.4 ns (Fig. 2(c)) as well as that of the shortening amplitude-average estimated lifetime from 3.6 ns down to 3.1 ns in the case of non-overlapping laser passes (and from 4.4 ns down to 3.8 ns in the case of multiple overlapping laser passes), as shown in Fig. 2(d) highlights the existence of an additional non-radiative de-excitation pathway for Ag_m^{n+} nanoclusters in presence of Yb^{3+} ions. Beyond the observation of a Ag_m^{n+} → Yb^{3+} energy transfer, it is of interest to go deeper in its origin. Förster resonant energy transfers (FRET) correspond to dipole-dipole energy transfers for which the radiative relaxation of an excited dipole (donor) is quenched in presence of a resonant dipole (acceptor)[46,47]. In this case, the relaxation oscillation of the dipolar moment of the donor leads to a non-radiative stimulation of the acceptor, providing the excitation of the acceptor while preventing the radiative emission of the donor. Such transfer occurs both for homo-dipole or hetero-dipole interactions, requiring only resonant energy levels[50]. Marasanov *et al.* have recently reported resonant energy transfers in a silver-containing photo-thermo-refractive (PTR) glass co-doped with Eu^{3+} ions[50]. FRET interactions are known to span over a few tens of nanometers (up to 20-30 nm), connecting donors and acceptors when spectral overlap exists between the donor emission and acceptor absorption spectra. In the recently investigated case of Eu^{3+}-doped PTR glass, Marasanov

et al. estimated the Förster distance to 0.4 nm[50]. We performed similar estimation in our previous work on Ag_m^{n+} → Eu^{3+} resonant energy transfer[44], leading to a the Förster distance to 1.1 nm. The 1.1 nm value from Petit *et al*. is slightly larger than the 0.4 nm from Marasanov *et al*. only because of the brighter laser-inscribed silver nanoclusters exhibiting a larger spectral emission overlap with Eu^{3+} absorption spectrum as compared to the silver nanoclusters existing in the pristine Eu^{3+} PTR glass. In the present case with the considered Yb^{3+}-doped silver-containing phosphate glass, Yb^{3+} shows no absorption in the visible range so that the spectral ranges of Yb^{3+} absorption (see Fig. S5) and Ag_m^{n+} emission (see Fig. 1(b)) do not overlap (at least extremely weakly) since the present silver nanocluster fluorescence drastically drops down beyond 800 nm. The Förster distance cannot be estimated, so that it tends to be a null distance. Thus, it appears that FRET interactions should be disregarded in the present case of Ag_m^{n+} → Yb^{3+} resonant energy transfer. This also implies that successive processes of silver nanocluster emission and subsequent Yb^{3+} absorption can be excluded too. The remaining reasonable transfer mechanism is thus Dexter energy transfer, being associated to an energy transfer mediated by a charge transfer from the donor to the acceptor when their wavefunctions overlap, which is still subject to interpretation depending on the considered glass matrix[19]. Therefore, in the case of energy transfers dominated by Dexter processes, it mostly restricts energy transfers to directly neighboring Yb^{3+} ions and laser-inscribed silver nanoclusters separated by one chemical bond. Based on the Ag-Yb phosphate glass composition, one estimates the initial inter-distances of 0.9 nm between fully dispersed Ag^+ ions and 15 nm between isolated Yb^{3+} ions. Because of the moderate laser inscription regime of Type A modifications compared to Type I[33] one can ensure that the direct laser-induced precipitation of plasmonic metallic silver nanoparticles is a minority effect in such an oxidative phosphate glass matrix so that any local plasmon field enhancement mechanisms shall be disregarded to play any dominant role here in the activation of near-IR fluorescence emission of Yb^{3+} ions[37,51,52]. Moreover, in such a Type A regime, large Yb^{3+} ions do not move so that their own inter-distance is maintained under the Type A laser/matter interaction regime. However, Desmoulin *et al*. had shown by X-ray photoelectron spectroscopy that laser inscription leads to the radial diffusion of silver elements with respect to the center of the voxel, providing a local reduction of about 10% of silver element concentration[53]. Such diffused silver elements contribute to the silver nanocluster creation and growth at the surrounding of the laser/glass interaction voxel, leading to silver nanocluster distributions with a

typical lateral width about a few hundreds of nanometers (200 to 300 nm[37], or possibly down to 80 nm[54]). In order to fix ideas, let's suppose that 100% of the mobile Ag^+ ions contribute to the formation of silver nanoclusters, and that the average nuclearity of Ag_m^{n+} is three silver elements. In such hypothesis, the localized silver nanocluster concentration typically corresponds to 0.05× $N_0^{Ag^+} \sim 0.5\times10^{20}$ cm^{-3}, with $N_0^{Ag^+} = 9.9\times10^{20}$ cm^{-3} (as given in Experimental Section and Table 1 of Alassani *et al.*)[43]. Although subject to hypotheses, such an estimation corresponds to 0.1× $N_0^{Yb^{3+}}$, which corroborates that there exists a non-negligible fraction of silver nanoclusters and Yb^{3+} ions in close vicinity with overlapping atomic orbitals compatible with the DEXTER energy transfer process.

2.3 Energy transfer based excitation of spatially-localized gain medium for laser amplification

Silver nanoclusters were inscribed along the full length of 1 cm long sample, leading to the creation of a highly stable waveguide since the molecular silver species induce a positive refractive index modification compatible by sustaining waveguiding behavior[32,48]. Indeed, this silver nanocluster sustained waveguides have shown exhibit excellent stability, versatile geometries, laser-induced losses down to 0.35±0.06 dB/cm and adapted mode profiles compatible with single-mode quasi-circular guided modes[30,32,33]. For the present inscription of the waveguide, a Zeiss 40× NA 0.75 objective has been used with laser irradiance about 4.05 TW.cm^{-2} and displacement velocity of 100 µm.s^{-2}. The waveguide was achieved with 16 forward and 16 return passes with a 250 nm line spacing to homogenize the refractive index change, giving access to an homogeneous square section with dimensions of 6×6 µm^2, similarly to what shown by Loi et al[30].

The waveguide showed single-mode propagation behavior at 1030 nm, whatever the achieved injection orientation at this wavelength. At 1030 nm, the intrinsic absorption of Yb^{3+} ions leads to a lineic losses of 1.1 dB/cm (see Supporting Information #E), while laser-induced structuring losses of the waveguide (due to material modifications) are in the range of 0.4±0.1 dB/cm. This leads thus to an overall waveguide attenuation of 1.5±0.1 dB/cm at 1030 nm (attenuation dominated by the rare earth absorption at 1030 nm). A 405 nm laser diode has been injected longitudinally into the waveguide so as to excite the donors (the silver nanoclusters), with an input UV power up to 12

mW. The local linear absorption coefficient α^{UV} at 405 nm in the considered waveguide is estimated to 10-20 cm^{-1}, typically corresponding to absorption losses of 43-86 dB/cm (see Supporting Information #F). The near-IR emission of Yb^{3+} ions has been collected at 1030 nm for stimulation powers from 28 mW up to 182 mW, as illustrated by Fig. 3(a). The co-injection of the two lasers and the collection of the amplified near-IR radiation were achieved with 10×-NA0.26 and 100×-NA0.7 microscope objectives at the input and output facets of the sample, respectively. For each stimulating power, the generated near-IR power showed a linear dependence with a gained near-IR extraction up to 1.2 mW with a UV injected power of 12 mW, corresponding to a 10% UV-to-IR net power conversion and a 25% UV-to-IR net photon conversion, as shown in Fig. 3(b). This linear behavior shows that the UV pumping process remains below absorption saturation regime for the silver nanoclusters. After normalizing the near-IR extracted powers (for the distinct UV pumping powers) by the near-IR transmitted power without UV pumping, Fig. 3(c) shows that all curves from Fig. 3(b) rescale identically so that the laser gain experiments correspond to "small signal" gain measurements with near-IR intensities well below the associated saturation intensity of the emission transition of the Yb^{3+} ions. Moreover, Fig. 3(c) shows up to a 7.3% near-IR amplification $\Delta P^{IR}/P^{IR}_{no\ UV} = (P^{IR}_{with\ UV} - P^{IR}_{no\ UV})/P^{IR}_{no\ UV}$, where $P^{IR}_{no\ UV}$ and $P^{IR}_{with\ UV}$ are near-IR output powers without and with UV pumping, respectively. Note that such a normalization of the measured output powers cancels out all the propagation losses of the waveguide as well as the injection coupling ratio, which makes these data free from any approximations. Figure 3(c) also shows an associated relative gain efficiency slope of 0.63±0.01 % per mW of UV pumping power in such a fully non-saturated configuration. The amplification factor corresponds to $G = P^{IR}_{with\ UV}/P^{IR}_{no\ UV} = 1 + \Delta P^{IR}/P^{IR}_{no\ UV} = e^{\Delta g_0 \cdot L^{UV}_{eff}}$. In a non-saturated configuration, it can therefore write $G = e^{\Delta g_0 \cdot L^{UV}_{eff}}$, where the relative "small signal" gain writes $\Delta g_0 = N_0^{Yb^{3+}} \beta(\sigma_{em.} + \sigma_{abs.})$, as detailed in Fig. S5. As the UV absorption follows a Beer-Lambert attenuation law, the resulting laser gain distribution along the waveguide bears the same longitudinal profile. Thus, the relevant effective length to be considered for amplification process here corresponds to $L^{UV}_{eff} = 1/\alpha^{UV}$, with α^{UV} the linear absorption coefficient of the waveguide at the UV pumping wavelength (namely at 405 nm). Here, the local linear absorption coefficient α^{UV} at 405 nm in the considered waveguide is estimated to 10-20 cm^{-1}, typically corresponding to an effective length L^{UV}_{eff} of 0.05-0.1 cm (see

Supporting Information #F). Such lengths are in reasonable agreement with the observed lengths of UV energy deposition along the waveguide. In this sense, the inversion population ratio β was extracted for the different UV pumping powers, with effective UV lengths from 0.05 to 0.15 cm, as shown in Fig. 3(d). Depending on the considered effective UV lengths – and thus on the effective volume where energy transfers occur along the waveguide – we report on experimental conditions where optically-induced transparency was achieved (see Fig. S5), with obtained inversion population ratios $\beta \geq \beta_{transp.}^{1030nm} = 8.5\%$. Such domains are shaded in purple and green for effective UV lengths of 0.05 and 0.15 cm, respectively, as shown in Fig. 3(d). These estimations comfort the interpretation that along the first millimeter of waveguide typically, we did achieve a laser-inscribed 3D-localized laser-gain medium based on the donor/acceptor pairs of silver nanoclusters and Yb^{3+}.

The demonstrated laser amplification at 1030 nm shows that the donor/acceptor pair (namely a nanocluster-Yb^{3+} pair) can act as a lasing hybrid system, similarly to other well-known systems such as Helium-Neon gas mixtures or Yb-Er doped amplification devices. Indeed, estimations reported in Fig. 3(d) suggest that the considered UV pumping of silver nanoclusters led to sufficient energy transfers towards Yb^{3+} ions to locally reach inversion population fractions so as to locally achieve optically-induced transparency and net laser gain amplification. This remarkable milestone means that laser inscription allows for the creation of 3D-localised hybrid laser active medium where such a laser gain distribution can be selectively excited with selective UV or visible excitation while the near-IR emitting acceptors are randomly distributed. Moreover, due to the strong linear absorption coefficient of silver nanoclusters and taking in account the coupling between nanoclusters and Yb^{3+} ions, one can possibly access indirect $Ag_m^{n+} \rightarrow Yb^{3+}$ excitation with similar efficiency compared to the standard Yb^{3+} direct pumping at 976 nm at the zero-phonon line. Besides, although the involved quantum defect is larger when considering the UV-VIS indirect pumping of the Yb^{3+} ions compared to the standard direct excitation at 976 nm at the zero-phonon line, one can note that the use of a donor/acceptor pair allows for the partial decoupling of the fluorescence lifetime features at excitation and emission, respectively. Indeed, indirect pumping of the Yb^{3+} ions mediated by energy transfers allows for excitation at an effective time scale that corresponds to the silver nanoclusters fluorescence lifetime (at the ns time scale) multiplied by the

mean number of spontaneous cycles of absorption/emission of silver nanoclusters needed to observe one energy transfer occurrence for a given nanocluster/Yb^{3+} pair. Since Yb^{3+} ions have a ms range fluorescence lifetime, the build-up time scale of the hybrid nanocluster/Yb^{3+} system may be faster than that of isolated Yb^{3+} ions.

The dependence of the resulting laser gain properties of the produced hybrid donor/acceptor complex with respect to laser irradiation parameters is of interest. Indeed, increasing the laser exposure parameters (larger intensity, larger amount of cumulated number on pulses thanks to a lower velocity) tends to increase the induced population of silver clusters. This tends thus to increase the associated absorption properties, increasing then the occurrence of energy transfers from excited silver clusters toward Yb^{3+} ions. In this case, the laser gain is expected to increase, by independently increase absorption properties of the donor (silver clusters) while keeping constant emission properties of the acceptor (Yb^{3+} ions that remain at a constant concentration). Moreover, while considering overlap between successive laser passes, this is less trivial. Indeed, by reducing the interlines between successive laser passes down to 250 nm, one achieves different silver nanocluster populations with different fluorescence properties with different absorption cross-sections. Thus, this can modify the absorption of the pumping energy by the nanoclusters and may influence the resulting laser gain properties. A more detailed analysis is beyond the scope of the present work. Moreover, our previous and numerous investigations on such silver-containing glasses have never show any noticeable changes in the Raman spectroscopy of this glass matrix in the laser-modified areas under our regime of irradiation[28]. No specific molecular oxygen has ever been observed in our case, so that potential laser-induced O defects shall be negligible here, thus with no significant influence of the performance of laser-created laser-gain medium.

Finally, further investigations will target the creation of integrated micro-lasers. As a consequence, higher powers for UV pumping are required, both for producing larger Yb^{3+} population inversions and also for achieving laser gain and amplification so as to compensate intra-cavity losses of the future integrated micro-lasers based of such co-doped photosensitive glasses. Such technological demand with higher UV pumping powers is reasonable nowadays while considering the ongoing development of multi-watt diodes in the UV and visible range needed for the excitation of the silver nanoclusters.

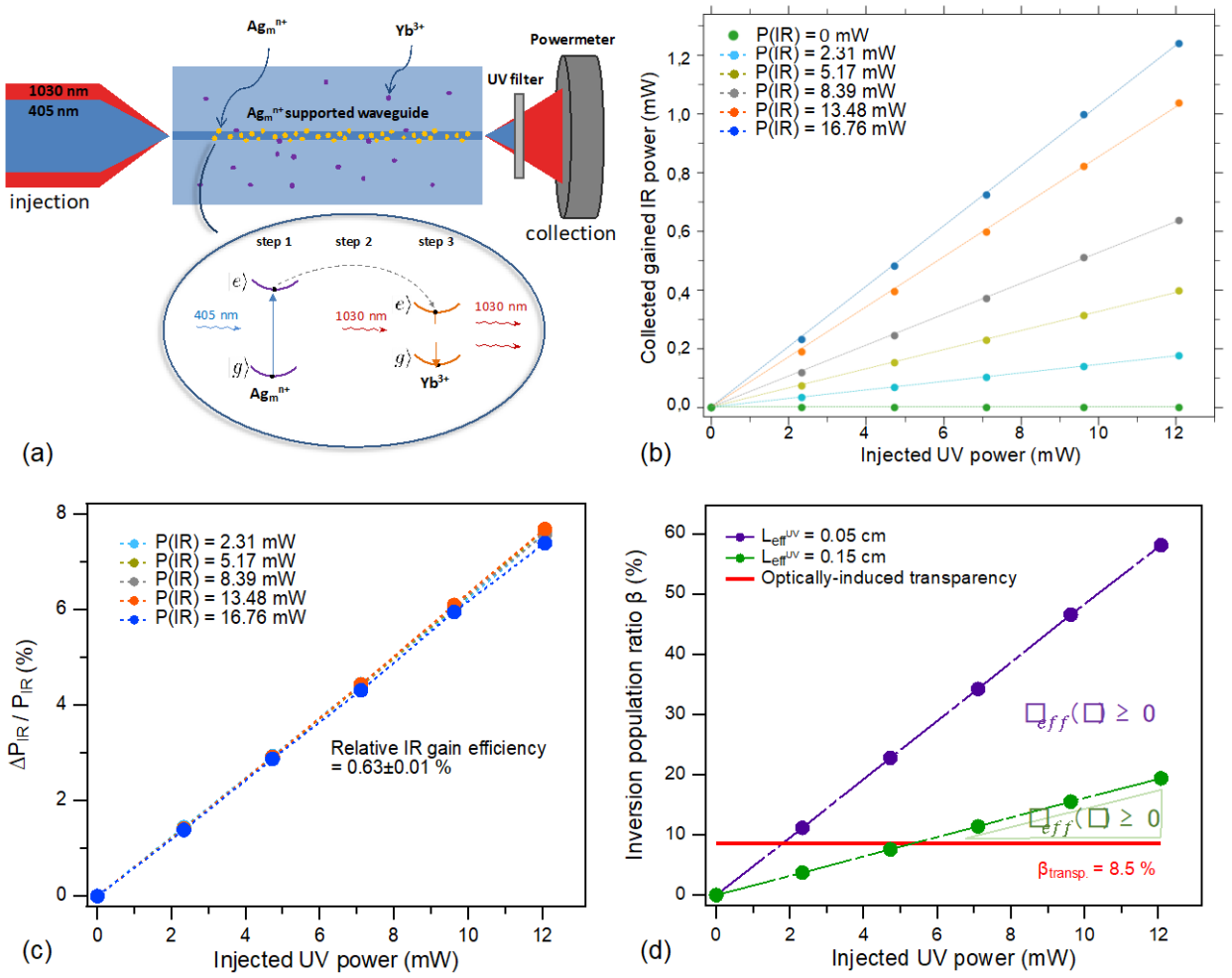

Figure 3. (a) Experimental scheme of longitudinal co-injection in a laser-inscribed silver nanocluster sustained waveguide of a pump beam (405 nm to selectively excite the silver nanoclusters acting as a donor) and a seed beam (1030 nm to selectively stimulate the near-IR emission of Yb^{3+} ions action as acceptor). Illustration of the involved spectroscopic scheme among the donor/acceptor pair. (b) Extracted absolute near-IR power and (c) relative near-IR amplification of the seed beam at 1030 nm versus UV pumping, respectively, for different stimulation powers. (d) Estimated Yb^{3+} inversion population fraction β versus UV pumping for boundary values of the effective UV absorption length, showing parameter configurations for which optically-induced transparency is achieved which thus leads locally to positive laser gain medium at 1030 nm.

3. Conclusion

We successfully reported on the femtosecond laser creation of highly fluorescent silver nanoclusters in an ytterbium-doped silver-containing phosphate glass. We furthermore demonstrated efficient energy transfer from the laser-inscribed silver nanoclusters towards the rare earth Yb^{3+} ions, leading to a near-IR background-free fluorescence emission. The laser-induced hybrid system composed of laser-inscribed silver nanoclusters and near-IR emitting Yb^{3+} ions

behaves as a pair of donor/acceptor, for which energy transfers are interpreted as a Dexter process between species with close orbital wavefunction overlapping. Since the donor emission and acceptor absorption spectral range show no overlapping, FRET-like energy transfers are excluded. In this framework, we demonstrated the 3D-localized near-IR emission of homogeneously-distributed Yb^{3+} ions thanks to the spatially-selective excitation of the laser-inscribed silver nanoclusters. Furthermore, the localized creation of hybrid pairs allowed for the creation of an effective 3D-distributed near-IR laser active medium in a laser-inscribed waveguide configuration by indirect pumping of Yb^{3+} ions. Effective laser gain was reported by the excitation of silver nanoclusters and the transfer to the Yb^{3+} lasing ions, with a UV-to-near-IR photon conversion yield up to 25%. Energy transfer based inversion population of the Yb^{3+} ions and associated optically-induced transparency is experimentally evidenced. Further work is needed to go beyond laser amplification and to achieve integrated laser devices, which requires both the creation of an active Fabry-Perot cavity[13] and pumping the silver nanocluster absorption with larger powers so that the achieved net laser gain compensates the cavity losses.

Such an approach allows for the conception and exploration of new lasing hybrid systems, compatible with the laser production of new laser active media especially for integrated laser-active waveguides. This includes perspectives of versatile 3D laser integrated architectures allowing for evanescent coupling under lasing operation with their environment, to achieve enhanced photonic sensing abilities beyond those offered by usual conventional planar of unidirectional architectures. Indeed, silver-sustained waveguides have already shown their remarkable potential for single-step surface laser inscription, giving a unique access to sensing ability over an extended range of refractive indices even down to those of aqueous solutions for biological sensing applications[48].

4. Experimental section

4.1 Glass preparation

Two photosensitive oxide glasses have been prepared from the standard melting-quenching technique (see the experimental section for the glass synthesis description), with the composition of $(100\text{-}x).[40P_2O_{5/2}\text{-}55ZnO\text{-}1Ga_2O_2\text{-}4Ag_2O] - x.Yb_2O_3$ (mol. %). For x = 0 and 0.8, the photosensitive glasses have been labeled PZnAg and PZnAg:Yb, respectively, the latter containing both silver photosensitive elements and fluorescent Yb^{3+} rare earth ions. Samples PZnAg and

PZnAg:Yb show very similar silver ion concentrations of $N_0^{Ag^+}$ = 10.2×10^{20} cm^{-3} and 9.9×10^{20} cm^{-3}, respectively, and a Yb^{3+} concentration of $N_0^{Yb^{3+}}$ = 5.6×10^{20} cm^{-3} for silver-Ytterbium phosphate. Both pristine samples showed the same silver ion spectroscopy, as reported elsewhere[39].

4.2 Direct infrared femtosecond laser writing

Laser inscription has been achieved in both the silver phosphate and silver-Ytterbium phosphate PZnAg and PZnAg:Yb samples, with the same two sets of laser irradiations (see the experimental section for the description of the femtosecond laser writing setup). Laser inscription was achieved while tightly focusing a femtosecond laser pulse train from a KGW:Yb femtosecond oscillator (9.8 MHz rep. rate, 1030 nm, pulse duration 400 fs, T-pulse 200 from Amplitude) combined with an acousto-optic modulator to control the number and the energy of pulses, thus enabling several irradiances. Spherical aberrations were mostly corrected in a versatile manner using a spatial light modulator (LCOS; X10468-03, Hamamatsu Photonics). A high-precision three-dimension translation stage XMS-50 (better than 50 nm resolution) was used to perform the sample positioning and displacements with various velocities including 10 µm.s^{-1} and 50 µm.s^{-1}. An Olympus microscope objective (20×, NA 0.75) was used to produce the photo-induced structures, 160 µm below the sample surface. Note that a frequency-doubled laser may be used but this approach was disregarded as irradiations at 515 nm lead to a higher probability to launch detrimental avalanche processes, which restricts the range of irradiance-velocity parameters. Moreover, we did not achieved significantly smaller features while considering the focusing of a 515 nm beam compared to a 1030 nm beam, mostly because of residual spherical aberrations due to the refractive index mismatch of our glass (around n = 1.59) compared to the ideal refractive index for which microscope objectives are designed for (around n = 1.518). Finally, high repetition rates are of high importance for the pulse-to-pulse cumulative process as the overall efficiency of silver nanocluster production depends on the delay between two successive pulses, to handle with the intermediate species Ag^0 with limited lifetimes at the microsecond scale[26].

4.3 Analysis of the photo-induced direct laser writing structures

Microluminescence was conducted with a LABRAM 800-HR spectrophotometer (Horiba Jobin-Yvon) and an Olympus microscope objective (50×, NA 0.75) using an excitation laser diode at 405 nm (100 mW, TEM00, OBIS, COHERENT). Microluminescence spectra were recorded thanks to

a thermoelectric cooled CCD Camera (Synapse Model 354308). The experimental spectra were corrected from the detection armresponse by a correction function determined using reference samples with broad spectral emission, while the pristine glass luminescence was subtracted from the recorded spectra.

Fluorescence lifetime imaging microscopy (FLIM) analysis was conducted using a Picoquant MT200 microscope equipped with two MPD single photon avalanche diodes (SPADs) and a PicoHarp300 timing board for time correlated single photon counting (TCSPC). The pulsed laser source was a LDH-D-C Picoquant pulsed laser diode at 375 nm, with a repetition rate set at 5 MHz and a typical pulse duration of 120 ps FWHM. The laser was mirrored to a 100× 1.40NA oil lens (UPLSAPO100XO, Olympus, Tokyo, Japan) by an 80%T/20%R spectrally flat beam splitter, and the later objective was also used for fluorescence collection. The fluorescence was transmitted through the same beam splitter, through a bandpass filter (D500/200m with a transmitted spectral window of 400-600 nm, Chroma Technologies, Rockingham, VT, USA) for elimination of excitation wavelength and then transmitted to the confocal optics and the detector. A piezoelectric stage was used for laser scanning. The presented FLIM images were calculated using the "FAST-FLIM" algorithm, in which for each pixel the reported lifetime was calculated as the first statistical moment of the single photon arrival time histogram distribution, minus a reference time taken at the beginning of the decay curve. Note that the FLIM images include temporal and intensity information of the collected fluorescence, as the colour code represents the average FAST-FLIM arrival times on the one hand and the brightness levels represent the number of collected events on the other.

4.4 Laser amplification metrology in laser-inscribed waveguides

Energy transfers investigated by means of both continuous and time-resolved micro-fluorescence imaging microscopy demonstrated indirect excitation of Yb^{3+} ions and resulting spontaneous emission. Stimulation emission such Yb^{3+} ions embedded in a hybrid acceptor/donor pair was investigated in a waveguided configuration. Laser inscription of waveguide was created in the PZn:4Ag-2Yb glass with the same setup described here above in Experimental Section *Direct infrared femtosecond laser writing*. The waveguide was achieved with 16 forward and 16 return passes with a 250 nm line spacing to homogenize the refractive index change, giving access to an homogeneous square section with dimensions of 6×6 μm^2. This waveguide was then placed in a

laser-gain pump/seed setup. A laser diode (405 nm, cw, OBIS, COHERENT) was injected through a 10× microscope objective (NA 0.28, Olympus) in the waveguide to excite the laser-inscribed silver nanoclusters that sustain the laser-inscribed waveguide. A tunable femtosecond Ti:sapphire laser (80 MHz, Chameleon, COHERENT) used at 1030 nm was then co-injected as a seed beam to stimulate the emission of Yb^{3+} ions and to observe laser gain. Collection was achieved with a 100× near-IR microscope objective (NA 0.7, Mitutoyo). Any residual pump power (405 nm) is filtered out after the collection microscope objective with a long pass filter, and the seed power (1030 nm) is measured using a *Thorlabs* power meter. For small gain values at both low UV pump and low seed powers, the power meter alone wasn't accurate enough, so we used a Lock-In detection system (SR830, Stanford Research Systems) to measure the gained infrared power (1030 nm). The laser diode pump power (405 nm) was modulated with a rotating wheel (ON/OFF modulation around 1 kHz), leading to the low-frequency modulation of silver nanocluster excitation and subsequent energy transfers to Yb^{3+} ions. The frequency of the wheel was sent to the Stanford Lock-In system for reference. The near-IR (1030 nm) output was collected with a photodiode whose signal was amplified and injected in the Lock-In system to filter out other frequencies than the reference frequency. This system enables accurate and high-sensitivity measurements at small signal levels in arbitrary units. The calibration in absolute power units was done carefully with the power meter when both the largest UV and seed powers were involved.

Funding: This research has benefited from financial support from French National Research Agency (ANR) ANR-19-CE08-0021-01, and from Région Nouvelle Aquitaine (project AAPR2020-2019-8193110). We acknowledge the financial support from the Grand Research Program « LIGHT » Idex University of Bordeaux, and the Graduate program « EUR Light S&T » PIA3 ANR-17-EURE-0027.

Author contributions : Not applicable.

Conceptualization, Y.P., T.C. and L.C.; methodology, Y.P., T.C. and L.C.; experimental validation & formal analysis, all authors; writing-original draft preparation, Y.P., F.A., T.C. and L.C.; writing-review and editing, all authors. All authors have read and agreed to the published version of the manuscript.

Institutional Review Board Statement: Not applicable.

Informed Consent Statement: Not applicable.

Data Availability Statement: Data underlying the results presented in this paper are not publicly available at this time but may be obtained from the authors upon reasonable request.

Supporting information files: the supporting information file contains five sections: **(A)** Spatial transverse profiles of laser-induced double-track fluorescent patterns for the UV excited silver nanoclusters (visible range) and for the indirectly excited Yb^{3+} ions by energy transfer from silver nanoclusters. **(B)** Resilience of the spatial homogeneity of the Yb^{3+} distribution fluorescence after fs laser inscription. **(C)** Time-resolved fluorescence decays of silver nanoclusters and influence of the co-insertion of Yb^{3+} ions, demonstrating lifetime shortening and energy transfers from the nanoclusters to the rare earth ions; **(D)** Visualization of the fitted parameters of Table 1, to show the overall consistency of the extracted set of parameters in the three-exponential decay model to depict the fluorescence lifetime decays of silver nanocluster patterns with and without the presence of Yb^{3+} ions. **(E)** Effective gain cross section depending on the population inversion rate of the lasing transition of the Yb^{3+} ions.

Acknowledgments: Not applicable.

Conflicts of Interest: The authors declare no conflict of interest.

REFERENCES

1. R. R. Gattass and E. Mazur, "Femtosecond laser micromachining in transparent materials," *Nat. Photonics* **2008**, 2(4), 219–225.
2. Ultrafast Laser Nanostructuring, The Pursuit of Extreme Scales. 2023. **Editors** R. Stoian, J. Bonse. Springer Series in Optical Sciences, Springer Cham. https://doi.org/10.1007/978-3-031-14752-4.
3. G. Corrielli, A. Crespi and R. Osellame, Femtosecond laser micromachining for integrated quantum photonics, *Nanophotonics* **2021**, 10(15), 3789–3812.
4. V. Tielen and Y. Bellouard, Three-Dimensional Glass Monolithic Micro-Flexure Fabricated by Femtosecond Laser Exposure and Chemical Etching, *Micromachines* **2014**, 5, 697-710. doi:10.3390/mi5030697.
5. M. Haque, K. K. C. Lee, S. Ho, L. A. Fernandes and P. R. Herman, Lab Chip **2014**, 14, 3817.
6. J. Thomas, C. Voigtländer, R.G. Becker, D. Richter, A. Tünnermann, and S. Nolte, Femtosecond pulse written fiber gratings: a new avenue to integrated fiber technology, *Laser Photonics Rev.* **2012**, 6(6), 709–723. / DOI 10.1002/lpor.201100033.
7. M. Bernier, D. Faucher, R. Vallée, A. Saliminia, G. Androz, Y. Sheng, and S. L. Chin, Bragg gratings photoinduced in ZBLAN fibers by femtosecond pulses at 800 nm, *Opt. Lett.* **2007**, 32(5), 454-456.
8. Lei et al., « Efficient ultrafast laser writing with elliptical polarization ». *Light: Science & Applications* **2023**, 12:74 https://doi.org/10.1038/s41377-023-01098-2.
9. Nelson G, Boehm U, Bagley S, et al. QUAREP-LiMi: A community- driven initiative to establish guidelines for quality assessment and reproducibility for instruments and images in light microscopy. *Journal of Microscopy*. 2021;*284:*56–73. https://doi.org/10.1111/jmi.13041.
10. S. Gross, N. Riesen, J. D. Love, and M. J. Withford, Three-dimensional ultra-broadband integrated tapered mode multiplexers, *Laser Photonics Rev.* **2014**, 8(5), 81–85. DOI 10.1002/lpor.201400078.
11. T. Meany, M. Gräfe, R. Heilmann, A. Perez-Leija, S. Gross, M. J. Steel, M. J. Withford, and A. Szameit, Laser written circuits for quantum photonics, *Laser Photonics Rev.* **2015**, 9(4), 363–384. **DOI** 10.1002/lpor.201500061.
12. M. Ams et al., *Nanophot*. **2017**, 6(5), 743-763. https://doi.org/10.1515/nanoph-2016-0119.
13. M. Ams , G. D. Marshall, P. Dekker, J. A. Piper and M. J. Withford, Ultrafast laser written active devices, *Laser & Photon. Rev*. **2009**, 3(6), 535–544. DOI 10.1002/lpor.200810050.

14. M. Karasek, Optimum design of Er^{3+}/Yb^{3+} codoped fibers for large-signal high-pump-power applications, IEEE Journal of Quantum Electronics **1997**, 33(10), 1699-1705. **DOI** 10.1109/3.631268.
15. H. Lin, D. Chen, Y. Yu, R. Zhang, et Y. Wang, « Molecular-like Ag clusters sensitized near-infrared down-conversion luminescence in oxyfluoride glasses for broadband spectral modification », *Appl. Phys. Lett.* **2013**, 103(9), 091902. doi: 10.1063/1.4819951.
16. R. Ma, J. Qian, S. Cui, X. Qiao, F. Wang, et X. Fan, « Enhancing NIR emission of Yb^{3+} by silver nanoclusters in oxyfluoride glass », *J. Lumin.* **2014**, 152, 222-225. **DOI** 10.1016/j.jlumin.2013.10.036.
17. V. K. Tikhomirov, T.Vosch, E. Fron, V. D. Rodríguez, J. J. Velázquez, D. Kirilenko, G. Van Tendeloo, J. Hofkens, M. Van der Auweraer and V. V. Moshchalkov « Luminescence of oxyfluoride glasses co-doped with Ag nanoclusters and Yb^{3+} ions », *RSC Adv.* **2012**, 2(4), 1496-1501. **DOI** 10.1039/C1RA01026C
18. H. Liao, S. Ye, R. Shen, X. Li, et D. Wang, « Effective formation of Ag nanoclusters and efficient energy transfer to Yb^{3+} ions in borosilicate glasses for photovoltaic application », *Mater. Res. Bull.* **2019**, 111, 113-117. **DOI**: 10.1016/j.materresbull.2018.10.042.
19. A. A. Amaro, G. Rodrigues da Silva Mattos, M. V. de Morais Nishimura, J. Dipold, N. U. Wetter and L. Reyes Pires Kassab, Silver Nanoclusters Tunable Visible Emission and Energy Transfer to Yb^{3+} Ions in Co-Doped GeO_2-PbO Glasses for Photonic Applications, *Nanomaterials* **2023**, 13, 1177. https://doi.org/10.3390/nano13071177.
20. Z. Guo, S. Ye, T. Liu, S. Li, et D. Wang, « SmF_3 doping and heat treatment manipulated Ag species evaluation and efficient energy transfer from Ag nanoclusters to Sm^{3+} ions in oxyfluoride glass », *J. Non-Cryst. Solids* **2017**, 458, 80-85. doi: 10.1016/j.jnoncrysol.2016.11.026.
21. J. A. Jiménez, S. Lysenko, H. Liu, et M. Sendova, « Luminescence of trivalent samarium ions in silver and tin co-doped aluminophosphate glass », *Opt. Mater.* **2011**, 33(8), 1215-1220. doi: 10.1016/j.optmat.2011.02.013.
22. R. Ma, J. Gao, Q. Xu, S. Cui, X. Qiao, J. Du, X. Fan « Eu^{2+} promoted formation of molecule-like Ag and enhanced white luminescence of Ag/Eu-codoped oxyfluoride glasses », *J. Non-Cryst. Solids* **2016**, 432, 348-353. doi: 10.1016/j.jnoncrysol.2015.10.032.
23. O. L. Malta, P. A. Santa-Cruz, G. F. De Sá, et F. Auzel, « Fluorescence enhancement induced by the presence of small silver particles in Eu^{3+} doped materials », *J. Lumin.* **1985**, 33, 3, 261-272. doi: 10.1016/0022-2313(85)90003-1.

24. Y. Shi, S. Ye, J. Yu, H. Liao, J. Liu, et D. Wang, « Simultaneous energy transfer from molecular-like silver nanoclusters to Sm^{3+}/Ln^{3+} (Ln = Eu or Tb) in glass under UV excitation », *Opt. Express* **2019**, 27(26), 38159-38167. doi: 10.1364/OE.380860.
25. J. M. Ward, D. G. O'Shea, B. J. Shortt, et S. N. Chormaic, « Optical bistability in Er-Yb codoped phosphate glass microspheres at room temperature », *J. Appl. Phys.* **2007**, 102(2), 023104. doi: 10.1063/1.2753591.
26. M. Bellec, A. Royon, K. Bourhis, J. Choi, B. Bousquet, M. Treguer, T. Cardinal, J-J. Videau, M. Richardson and L. Canioni1 « 3D Patterning at the Nanoscale of Fluorescent Emitters in Glass », *J. Phys. Chem. C* **2010**, 114(37), 15584-15588. doi: 10.1021/jp104049e.
27. P. Kunwar and P. Soman, Direct Laser Writing of Fluorescent Silver Nanoclusters: A Review of Methods and Applications A*CS Appl. Nano Mater*. **2020**, 3, 7325−7342. doi:10.1021/acsanm.0c01339
28. Y. Petit, S. Danto, T. Guérineau, A. Abou Khalil, A. Le Camus, E. Fargin, G. Duchateau, J-P. Bérubé, R. Vallée, Y. Messaddeq, T. Cardinal and L. Canioni « On the femtosecond laser-induced photochemistry in silver-containing oxide glasses: mechanisms, related optical and physico-chemical properties, and technological applications », *Adv. Opt. Technol.* **2018**, 7(5), 291-309. doi: 10.1515/aot-2018-0037.
29. E . Smetanina, B. Chimier, Y. Petit, N. Varkentina, E. Fargin, L. Hirsch, T. Cardinal, L. Canioni and G. Duchateau « Modeling of cluster organization in metal-doped oxide glasses irradiated by a train of femtosecond laser pulses », *Phys. Rev. A* **2016**, 93(1), 013846. doi: 10.1103/PhysRevA.93.013846.
30. L. Loi, Y. Petit and L. Canioni, *High refractive index change in Type A laser modification using a multi-scan approach*. Opt. Mat. Express **2022**,12, 2297–2308. doi:10. 1364/ome.457655.
31. R. Laberdesque, L. Loi, T. Guérineau, S. Danto, T. Cardinal, L. Canioni, and Y. Petit, *Three-dimensional femtosecond laser inscription of Type-A based high-efficiency first-order waveguide Bragg gratings*, Adv. Opt. Technol. – Applied Photonics, volume 12 (2023). doi: 10.3389/aot.2023.1237679
32. A. Abou Khalil, J-P. Bérubé, S. Danto, J-C. Desmoulin, T. Cardinal, Y. Petit, R. Vallée and L. Canioni « Direct laser writing of a new type of waveguides in silver containing glasses », *Sci. Rep.* **2017**, 7(1), 1. doi: 10.1038/s41598-017-11550-0.
33. A. Abou Khalil, J-P. Bérubé, S. Danto, T. Cardinal, Y. Petit, R. Vallée and L. Canioni « Comparative study between the standard type I and the type A femtosecond laser induced

refractive index change in silver containing glasses », *Opt. Mater. Express* **2019**, 9(6), 2640-2651. doi: 10.1364/OME.9.002640.

34. K.-I. Kawamura, M.Hirano, T. Kurobori, D. Takamizu, T. Kamiya, and H. Hosono, Femtosecond-laser-encoded distributed-feedback color center laser in lithium fluoride single crystals, Appl. Phys. Lett. **84**(3), 311-313 (2004).
35. B. G. Ershov, E. Janata, et A. Henglein, « Growth of silver particles in aqueous solution: long-lived "magic" clusters and ionic strength effects », *J. Phys. Chem.* **1993**, 97(2), 339-343. doi: 10.1021/j100104a013.
36. R. Espiau de Lamaestre, H. Béa, H. Bernas, J. Belloni, et J. L. Marignier, « Irradiation-induced Ag nanocluster nucleation in silicate glasses: Analogy with photography », *Phys. Rev. B* **2007**, 76(20), 205431. doi: 10.1103/PhysRevB.76.205431.
37. N. Marquestaut, Y. Petit, A. Royon, P. Mounaix, T. Cardinal, et L. Canioni, « Three-Dimensional Silver Nanoparticle Formation Using Femtosecond Laser Irradiation in Phosphate Glasses: Analogy with Photography », *Adv. Funct. Mater.* **2014**, 24(37), 5824-5832. doi: 10.1002/adfm.201401103.
38. F. Alassani, J.-C. Desmoulin, O. Cavani, Y. Petit, T. Cardinal, N. Ollier, Silver, Photochemical reactivity under electronic irradiation of Zinc phosphate and, Sodium Gallo-phosphate glasses, J. Non Cryst. Solids 600, 122009 (2023).
39. A. Royon, K. Bourhis, M. Bellec, G. Papon, B. Bousquet, et al., Adv. Mater. 22, 5282–5286 (2010)).
40. A. Royon et al, Durability study of a fluorescent optical memory in glass studied by luminescence spectroscopy, Microelectronics Reliability 53 (2013) 1514–1518.
41. V. Jubera, J. Sablayrolles, F. Guillen, R. Decourt, M. Couzi, et A. Garcia, « From the infrared to the visible range: Spectroscopic studies of Ytterbium doped oxyborates », *Opt. Commun.* **2009**, 282(1), 53-59. doi: 10.1016/j.optcom.2008.09.075.
42. T.T. Fernandez, M. Sakakura, S.M. Eaton, B. Sotillo, J. Siegel, J. Solis, Y. Shimotsuma, K. Miura, "Bespoke photonic devices using ultrafast laser driven ion migration in glasses", *Progress in Materials Science* **2018**, 94 68–113. https://doi.org/10.1016/j.pmatsci.2017.12.002
43. F. Alassani, G. Galleani, G. Raffy, A. Del Guerzo , A. Royon , K. Bourhis, A. S. Stucchi de Camargo, V. Jubera, L. Canioni, T. Cardinal, Y. Petit, "Direct laser writing of visible and near infrared 3D luminescence patterns in glass" (INVITED), *Optical Materials: X* **2022**, 16 100205, 1-10.
44. Y. Petit, G. Galleani, G. Raffy, J.-C. Desmoulin, V. Jubera, A. Guerzo, A.S.S. de Camargo, L. Canioni, T. Cardinal, « three-dimensional high spatial localization of efficient resonant energy

transfer from laser-assisted precipitated silver clusters to trivalent europium ions », *Crystals* **2021**, 11(2), 1-16. https://doi.org/10.3390/ cryst11020148.

45. K. Bourhis, A. Royon, M. Bellec, J. Choi, A. Fargues, M. Treguer, J-J. Videau, D. Talaga, M. Richardson, T. Cardinal, L. Canioni « Femtosecond laser structuring and optical properties of a silver and zinc phosphate glass », *J. Non-Cryst. Solids* **2010**, 356(44), 2658-2665. doi: 10.1016/j.jnoncrysol.2010.03.033.
46. S.E. Braslavsky, E. Fron, H.B. Rodríguez, E.S. Román, G.D. Scholes, G. Schweitzer, B. Valeur and J. Wirz, *Photochem. Photobiol. Sci.* **2008**, **7**, 1444–1448.
47. I. Medintz and N. Hildebrandt, *FRET – Förster Resonance Energy Transfer*, Wiley-VCH Verlag GmbH & Co. KGaA, Weinheim, 2014.
48. A. A. Khalil, P. Lalanne, J-P. Bérubé, Y. Petit, R. Vallée and L. Canioni « Femtosecond laser writing of near-surface waveguides for refractive-index sensing », *Opt. Express* **2019**, 27(22), 31130-31143. doi: 10.1364/OE.27.031130.
49. K. Bourhis, A. Royon, G. Papon, L. Canioni, N. Makria, Y. Petit, T. Cardinal, Luminescence properties of micrometric structures induced by direct laser writing in silver containing phosphate glass, *J. of Non-Cryst. Solids* **2013**, 377, 142–145.
50. D. V. Marasanov, L. Yu. Mironov, Y. M. Sgibnev, I. E. Kolesnikov and N.V. Nikonorov, "Luminescence and energy transfer mechanisms in photo-thermo-refractive glasses co-doped with silver molecular clusters and Eu^{3+}", Phys. *Chem. Chem. Phys.* **2020**. DOI: 10.1039/d0cp02786c
51. M. Eichelbaum et K. Rademann, « Plasmonic Enhancement or Energy Transfer? On the Luminescence of Gold-, Silver-, and Lanthanide-Doped Silicate Glasses and Its Potential for Light-Emitting Devices », *Adv. Funct. Mater.* **2009**, 19(13), 2045-2052. doi: 10.1002/adfm.200801892.
52. J. R. Lakowicz, « Radiative decay engineering 5: metal-enhanced fluorescence and plasmon emission », *Anal. Biochem.* **2005**, 337(2), 171-194. doi: 10.1016/j.ab.2004.11.026.
53. J-C. Desmoulin, Y. Petit, L. Canioni, M. Dussauze, M. Lahaye, H. M. Gonzalez, E. Brasselet and T. Cardinal « Femtosecond laser structuring of silver-containing glass: Silver redistribution, selective etching, and surface topology engineering », *J. Appl. Phys.* **2015**, 118, 213104. doi: 10.1063/1.4936233.
54. M. Bellec, A. Royon, B. Bousquet, K. Bourhis, M. Treguer, et al., "Beat the diffraction limit in 3D direct laser writing in photosensitive glass", Opt. Express **2009**, 17, 10304–10318.

Graphic for manuscript